Records of Extreme Ground Accelerations during the 2011 Christchurch Earthquake Sequence Contaminated by a Nonlinear, Soil–Structure Interaction

Hiroyuki Goto*[1], Yoshihiro Kaneko[2,3], Muriel Naguit[3], and John Young[3]

ABSTRACT

Ground-motion records are critical for seismic hazard assessment and seismic design of buildings and infrastructures. Large (> 1*g*), asymmetric vertical accelerations (AsVAs) have been observed at strong-motion stations during recent earthquakes. However, it is not clear whether all of the observed AsVAs reflect actual ground shaking or the interaction of a building structure and underlying ground. Here, we investigate the cause of large AsVAs recorded at several seismic stations in Christchurch, New Zealand, during the 2011 M_w 6.2 Christchurch earthquake. We first define three metrics and quantify the degree of waveform asymmetry in all available records from nearby $M > 3$ earthquakes. Histograms of the metrics show greater waveform asymmetry for larger accelerations at these stations, which is consistent with the prediction of a nonlinear, soil–structure interaction associated with the elastic collisions of a foundation slab onto the underlying soil. We then use finite-element models to examine the occurrence of the nonlinear, soil–structure interaction at these stations during the M_w 6.2 mainshock and M_w 5.6 aftershock of the 2011 Christchurch earthquake. The parameters of the numerical models are constrained by site investigation of selected stations. We find that numerical simulations closely reproduce the large AsVAs recorded at stations HVSC and PRPC, suggesting that these ground-motion records were contaminated by the nonlinear, soil–structure interaction. Seismic sensors located near the corner of a concrete slab are shown to be more prone to this phenomenon. Our results further suggest that artificial recording of large AsVAs due to the nonlinear, soil–structure interaction can be mitigated if a seismic sensor is placed closer to the center of a foundation slab. The analytical procedure presented in this study may be useful in identifying the occurrence of AsVAs elsewhere and in assessing whether AsVAs are caused by the nonlinear, soil–structure interaction.

KEY POINTS

- Large, asymmetric vertical accelerations have been observed at strong-motion stations during recent earthquakes.
- We performed finite-element analysis of station responses using model parameters constrained by our site survey.
- Simulations closely reproduce the records, suggesting contamination by nonlinear, soil–structure interaction.

INTRODUCTION

Large ground accelerations exceeding gravitational acceleration (1*g*) have been recorded from previous earthquakes; for example, the 1976 Gazli earthquake (U.S. Geological Survey [USGS], 1976), the 1979 Imperial Valley earthquake (Porcella and Matthiesen, 1979), the 1994 Northridge earthquake (Shakal *et al.*, 1994), the 2004 Chuetsu earthquake (Honda *et al.*, 2005), and the 2004 Rumoi earthquake (Maeda and Sasatani, 2009). Anderson (2010) provided the summary of 35 waveform records exceeding 1*g* acceleration from various earthquakes that occurred up to the summer of 2007 and discussed the statistical property of these ground motions.

1. Disaster Prevention Research Institute, Kyoto University, Kyoto, Japan; 2. Graduate School of Science, Kyoto University, Kyoto, Japan; 3. GNS Science, Lower Hutt, New Zealand

*Corresponding author: goto@catfish.dpri.kyoto-u.ac.jp

Cite this article as Goto, H., Y. Kaneko, M. Naguit, and J. Young (2021). Records of Extreme Ground Accelerations during the 2011 Christchurch Earthquake Sequence Contaminated by a Nonlinear, Soil–Structure Interaction, *Bull. Seismol. Soc. Am.* **XX**, 1–19, doi: 10.1785/0120200337

Since then, larger accelerations have been recorded during the 2008 Mogul earthquake (Anderson *et al.*, 2009), the 2008 Iwate–Miyagi earthquake (Aoi *et al.*, 2008), the 2011 Tohoku earthquake (Goto and Morikawa, 2012), and the 2018 eastern Iburi earthquake (Dhakal *et al.*, 2019). These large acceleration records contribute to the estimation of seismic hazard potential and the seismic loadings for engineering designs of buildings and infrastructures.

Among these earthquake events, there are cases in which the large accelerations are likely due to the local response at the location where the seismic sensor was situated. Ohmachi *et al.* (2011) examined the origin of large, asymmetric vertical accelerations (AsVAs) with a peak value of 3.9*g*, recorded at seismic station IWTH25 during the 2008 Iwate–Miyagi earthquake in Japan, and argued that the rocking motions of a shed where the sensor was installed induced the large positive accelerations upon the impact of the structural base on the soil ground. Goto *et al.* (2019) suggested that large AsVAs with a peak value of 3.2*g* at seismic station WTMC during the 2016 M_w 7.8 Kaikōura earthquake in New Zealand were caused by a flapping effect, that is, the local elastic bouncing of a foundation slab on which the sensor is installed. Both of these effects can be classified under a similar category of nonlinear, soil–structure interactions that involve the impact of a structural base on the underlying soil ground. Here, we refer to these effects as soil–structure collisions.

Soil–structure interactions have been well discussed in the field of earthquake engineering (Robertson, 1966; Jennings and Bielak, 1973; Bielak, 1974; Veletsos and Meek, 1974; Kausel, 2010). Numerous studies have concluded that soil–structure interactions can filter out the higher-frequency components of input motions due to spatial averaging (Hoshiya and Ishii, 1983; Luco and Wong, 1986; Kim and Stewart, 2003; Sotiriadis *et al.*, 2019). In contrast, Ohmachi *et al.* (2011) and Goto *et al.* (2019) pointed out a different situation in which the higher-frequency components can be enhanced by soil–structure collisions.

Previous studies (Ohmachi *et al.*, 2011; Goto *et al.*, 2019) suggest that large acceleration records may not always reflect actual ground motions and that AsVAs may be used to distinguish artificial signals from the actual ground motions. Both of the vertical accelerations recorded at stations IWTH25 and WTMC show clear asymmetries. The downward negative acceleration is limited to approximately gravitational acceleration (1*g*), whereas the upward positive acceleration greatly exceeds the gravitational acceleration. Examining the origin of large AsVAs observed elsewhere and assessing whether these records reflect actual ground motions are important for both the fundamental understanding of the nature of earthquake ground shaking and seismic hazard.

During the 2011 Christchurch earthquake sequence in New Zealand, large AsVAs were recorded at several stations. The records have been attributed to the evidence of the soil trampoline effect (Fry *et al.*, 2011), in which a rebound force causes a large upward acceleration and a downward motion is limited at the gravitational acceleration (1*g*) due to the bouncing of a deformable soil (Aoi *et al.*, 2008). Figure 1a shows seismic stations HVSC and PRPC, which are located close to the epicenter in Christchurch. The peak vertical acceleration of 2.2*g* at station HVSC and 1.9*g* at station PRPC were recorded, and these vertical accelerations show clear asymmetry (Fig. 1b). The downward accelerations are limited to approximately 1*g*, whereas the maximum value appeared in the upward direction (Fig. 1b). Station CCCC also recorded AsVAs; however, the asymmetrical characteristic is not as clear compared with stations HVSC and PRPC (Fig. 1b). Stations CBGS and SHLC did not show any asymmetry in the waveforms despite exceeding 0.1*g* in peak accelerations (Fig. 1b).

In this study, we examine waveform records at selected stations and assess whether the observed AsVAs were induced by the local system responses or actual ground motions. We take a comprehensive approach by analyzing and quantifying the asymmetry in waveform records, conducting station site surveys, and performing numerical simulations to quantify the station responses. We then discuss the implications of our results and strategies to mitigate the AsVAs.

QUANTIFICATION OF AsVAs RECORDS

Although large (>1*g*), AsVAs are visually identifiable, such as the HVSC and PRPC records during the mainshock of the 2011 M_w 6.2 Christchurch earthquake, evaluating AsVAs in weaker (<1*g*) ground-motion records has been largely subjective. To objectively assess the occurrence of AsVAs in weaker motions, we define several metrics to quantify the degree of waveform asymmetry and to evaluate the presence of AsVAs at strong-motion stations.

Previous numerical simulations of the elastic flapping effect (Goto *et al.*, 2019) suggest that the presence of AsVAs depends on the setup and installation conditions of a seismometer. The waveform asymmetry caused by soil–structure collisions is enhanced when the input ground motion is larger. Therefore, stations susceptible to the flapping effect would show a systematic bias in asymmetry characteristics in the waveform records.

In our analysis, we use the data from six seismic stations located in Waiau and Christchurch (Fig. 1a). Waveform records for all earthquakes greater than *M* 3.0, with epicenters within a 1.5° radius are used and are represented by black dots in Figure 1a.

To quantify the degree of asymmetry in vertical acceleration waveforms, Aoi *et al.* (2008) proposed a metric based on positive and negative envelopes. In this article, we modify this metric and define a similar quantity as follows:

$$Fs = \frac{|S^+| - |S^-|}{\max(|S^+|, |S^-|)}, \tag{1}$$

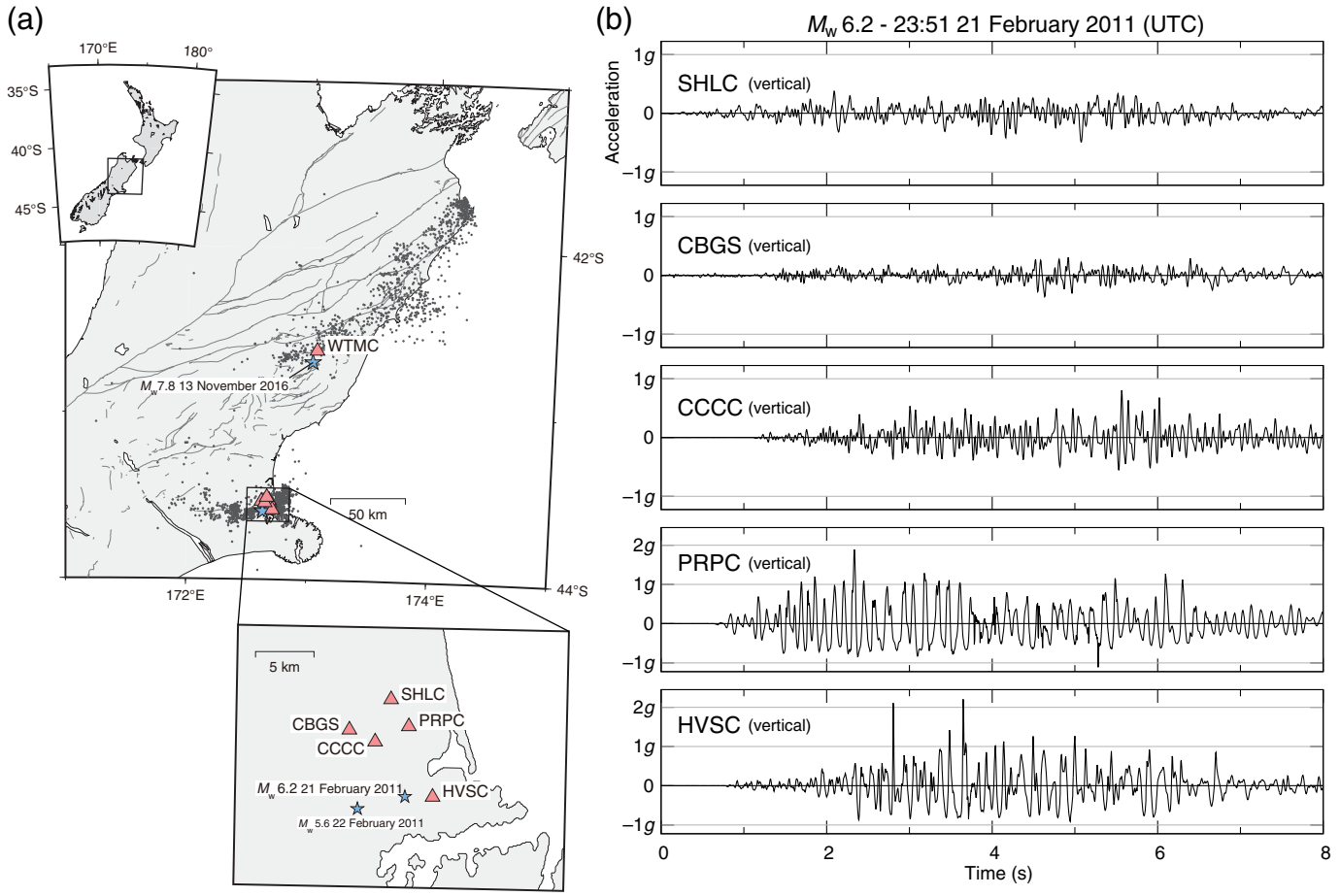

Figure 1. (a) Location of seismic station WTMC in Waiau and stations HVSC, PRPC, CCCC, CBGS, and SHLC in Christchurch, New Zealand. WTMC recorded large, asymmetrical vertical accelerations (AsVAs) during the 2016 M_w 7.8 Kaikōura earthquake. The Kaikōura earthquake's epicenter is denoted by a solid star. HVSC and PRPC recorded peak accelerations of 2.2*g* and 1.9*g*, respectively, during the 2011 M_w 6.2 Christchurch earthquake with the epicenter denoted by the solid star. Black dots denote epicenters of $M > 3.0$ earthquakes used to generate histograms shown in Figure 2. (b) Vertical acceleration waveforms recorded at HVSC, PRPC, CCCC, CBGS, and SHLC during the 2011 M_w 6.2 Christchurch earthquake. Asymmetry in the waveform records can be seen at HVSC, PRPC, and CCCC. The color version of this figure is available only in the electronic edition.

in which S^+ and S^- are the positive and negative envelopes, respectively, estimated from the linear interpolation of peak values. These envelopes are different from symmetric envelopes obtained from the Hilbert transform. Fry *et al.* (2011) proposed a different metric defined by the positive and negative peak values of vertical accelerations, as follows:

$$Fp = \frac{|P^+| - |P^-|}{\max(|P^+|, |P^-|)}, \tag{2}$$

in which P^+ and P^- are the positive and negative peak values, respectively.

Fs may be biased by the asymmetrical background noise before or after an earthquake-induced AsVA. *Fp* focuses only on the maximum value independent of frequency content and may be biased by the transient phenomena unrelated to the overall waveform asymmetry. To partially remedy these biases, we define another metric that accounts for several significant waveform peaks:

$$Fh = \frac{|H^+| - |H^-|}{\max(|H^+|, |H^-|)}, \tag{3}$$

in which H^+ is the average value of positive peaks exceeding 50% of the maximum value, whereas H^- is the average value for negative peaks. H^- is calculated using the same number of negative peaks used in H^+.

Figure 2 shows the histograms of *Fs*, *Fp*, and *Fh* for waveform records at selected stations. Colored histograms in Figure 2 indicate earthquake waveforms exceeding a peak ground acceleration (PGA) of 0.1*g* (blue) and 0.4*g* (red), respectively. Histograms for station WTMC show a clear shift in the positive direction (i.e., more positive asymmetry) for larger PGAs. This is consistent with the characteristics associated with the flapping effect (Goto *et al.*, 2019). The classical trampoline effect (Aoi *et al.*, 2008) cannot explain the positive

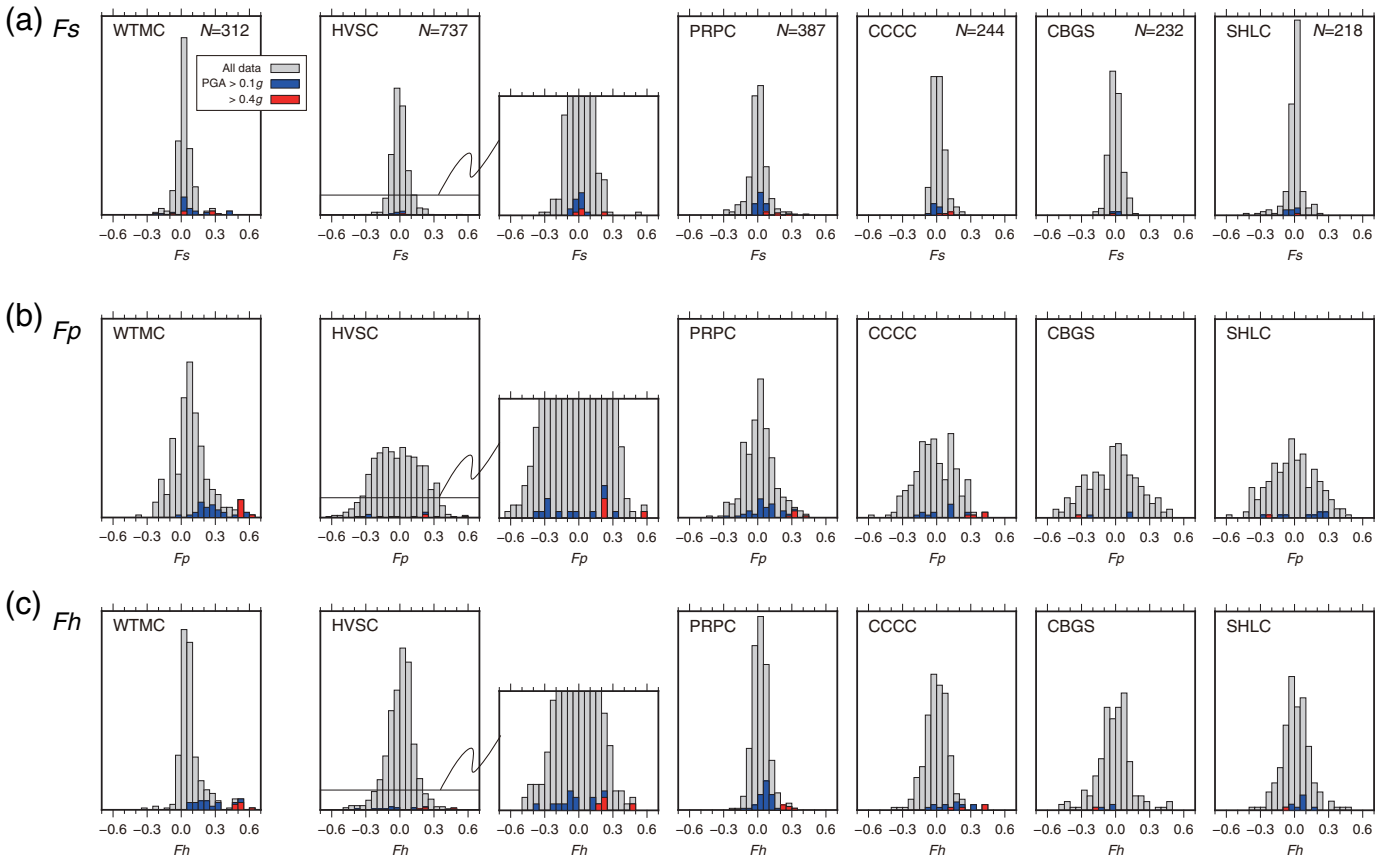

Figure 2. Histograms showing the degree of asymmetry in the vertical-component waveform records. Three metrics (a) *Fs*, (b) *Fp*, and (c) *Fh* are defined in the QUANTIFICATION OF AsVAs RECORDS section. The gray background represents all waveform data, whereas blue and red histograms highlight the waveform data exceeding a peak ground acceleration (PGA) of 0.1*g* and 0.4*g*, respectively. WTMC, HVSC, PRPC, and CCCC show a high degree of waveform asymmetry, especially for larger PGAs, whereas CBGS and SHLC do not indicate any asymmetry. The color version of this figure is available only in the electronic edition.

shift in the histogram for data not exceeding 1*g*. Similar positive shifts are also visible for metrics *Fp* and *Fh* as depicted in Figure 2. Stations PRPC and CCCC show similar trends as observed in WTMC. This suggests that strong-motion records at PRPC and CCCC may be contaminated by soil–structure collisions (Ohmachi *et al.*, 2011; Goto *et al.*, 2019). In contrast, CBGS and SHLC show no clear differences in the background and colored histograms, as shown in Figure 2. For HVSC, histograms do not clearly show a positive shift, but the data exceeding 0.4*g* are within the positive range for *Fp* and *Fh* (Fig. 2).

STATION SITE INVESTIGATION

To examine the site conditions at HVSC, PRPC, and CCCC and constrain the numerical model parameters, we surveyed the site and the installation conditions of acceleration sensors at the selected stations, including CBGS and SHLC, that do not show AsVAs. All of these stations are located in Christchurch, New Zealand, as shown in Figure 1a.

The acceleration sensor at HVSC is installed in a shed at a school in Heathcote Valley (Fig. 3). The sensor is contained in a protective outer enclosure (sensor box) and installed in a corner of a concrete foundation in the shed (Fig. 3b). The shed connects to the school hall, which is supported by five timber frames. The slab thickness is approximately 27 cm, which was measured by digging a hole beside the sensor location. We observed the presence of minor (<5 mm thick) gaps between the soil ground and the outer ring slab, which extends up to the foundation slab (Fig. 3c). The plan view and cross-section view, shown in Figure 3d–f, along the S64°E–N64°W direction depict the dimensions and setup of the site in detail. The shed is built with wood panels and corrugated iron walls.

The seismic sensor at station PRPC is installed in a shed at a pumping station located in Linwood (Fig. 4). The sensor box is placed at the southwestern corner of the shed (Fig. 4c). The slab on which the sensor rests has a thickness of 13 cm. Figure 4c–e shows the plan view and cross-section view. The shed is built with concrete masonry, and a partition wall is placed in the middle (Fig. 4c,d). The installation condition and dimensions of the sensor and sensor box are the same as those at station HVSC. No obvious gap between the soil

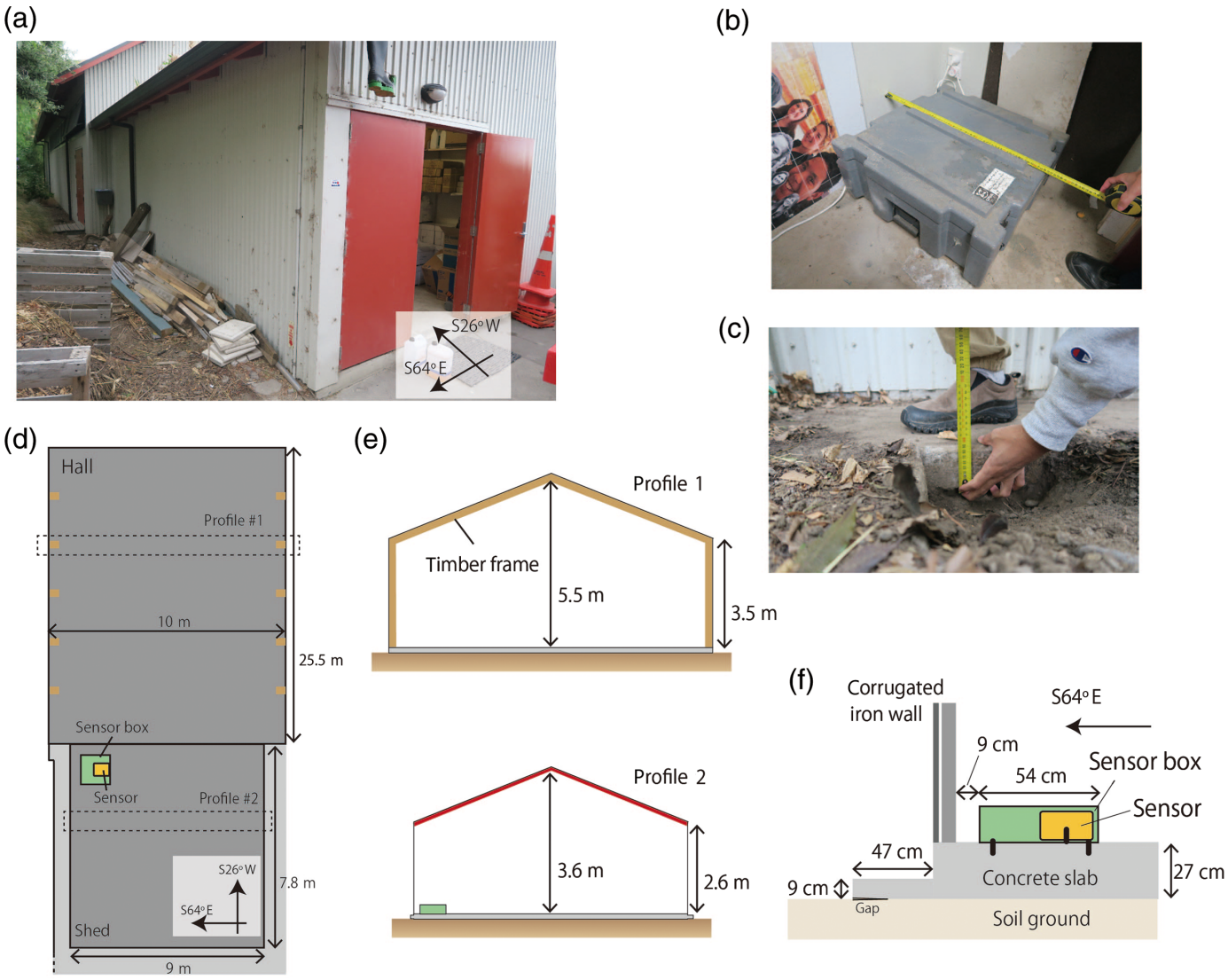

Figure 3. Installation conditions at HVSC. Photo of (a) exterior view, (b) sensor box, and (c) gap beneath the outer concrete slab. (d) Plan view and (e,f) cross-section views along the S64°E direction. The color version of this figure is available only in the electronic edition.

ground and the foundation slab is observed during the site visit.

Unlike HVSC and PRPC wherein the sensors are housed in a shed, the seismic sensor in CCCC is situated in the main structure of a school building in Christchurch central (Fig. 5a). The plan view and cross-section view are shown in Figure 5c–e. The sensor box is situated at a corner of a concrete foundation in a small room under the stairs (Fig. 5b). The building is a two-story structure, which is built with brick masonry. The foundation has a slab thickness of 15 cm. Similar to PRPC, there is no obvious gap between the soil ground and the foundation slab.

The strong-motion recorders deployed in stations HVSC, PRPC, and CCCC are CUSP3B models (Canterbury Seismic Instruments). This seismic recorder has a weight of 3.1 kg and dimensions of 28 cm by 26 cm by 13 cm. The sensor box enclosing the sensor, cables, and batteries weighs approximately 37 kg, with dimensions of 55 cm by 55 cm by 25 cm. The waveform records from these stations have a sampling frequency of 200 Hz. These seismic recorders are firmly connected to the sensor boxes, and the boxes are firmly anchored to the concrete slab.

NUMERICAL SIMULATION OF STATION RESPONSE

We conduct numerical simulations of station responses to better understand the origin of large AsVA records at stations HVSC, PRPC, and CCCC during the mainshock of the 21 February 2011 (UTC) M_w 6.2 Christchurch earthquake and the M_w 5.6 aftershock that occurred on 22 February 2011 (UTC). We examine the finite-element models used to simulate dynamic interactions between the concrete foundation slab and underlying soil. The detailed dimensions of the concrete

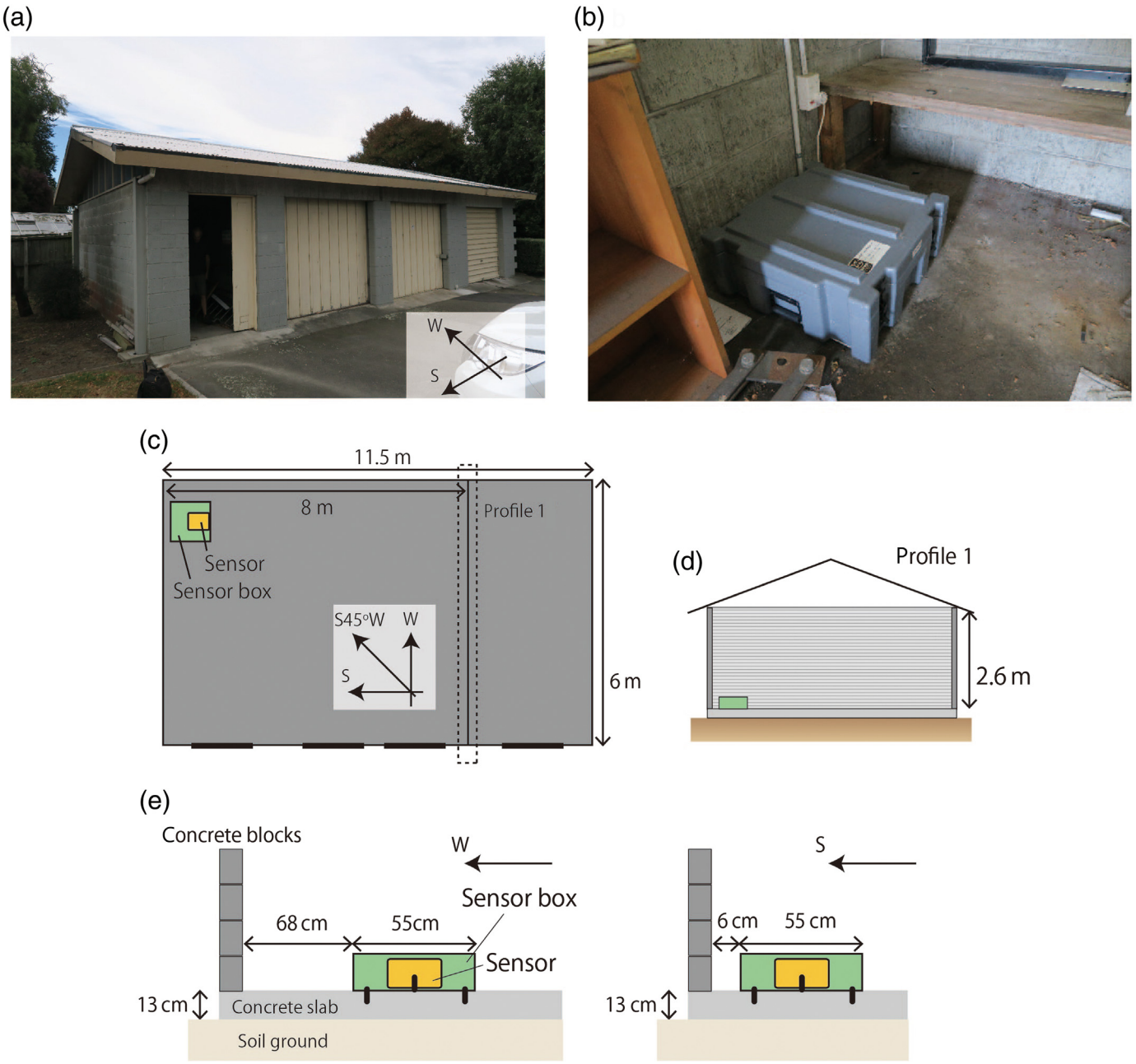

Figure 4. Installation conditions at PRPC. Photo of (a) exterior view and (b) sensor box. (c) Plan view and (d,e) cross-section views. The color version of this figure is available only in the electronic edition.

slab and sensor locations obtained from our site surveys are reflected in the numerical models.

Figure 6 shows the model setup. We create equivalent 2D models considering the upper structures. For HVSC, we take a S64°E–N64°W profile in the modeling. The five timber frames and two lateral solid walls (numbers 1 and 2) are incorporated in the model. The former solid wall is associated with the hall, and the latter wall is with the shed. For PRPC, we take a S45°W–N45°E profile to enhance the bouncing at the edge. Assuming that the stiffness of the wall structure is dominant in the vibration modes of the upper structure, the walls consisting of concrete blocks are modeled. For CCCC, we take a N19°E–S19°W profile. The brick lateral walls are integrated as solid walls in the model. The floor and roof slabs are incorporated. The detail profile and physical properties are summarized in Tables 1–3.

Each model includes a thin gap beneath the slab that represents irregular contacts between the slab and the underlying soil (Fig. 6). At HVSC, a minor gap of <5 mm is identified beneath the slab edge at HVSC (Fig. 3). Although no obvious gaps between the slab and underlying soil are observed at PRPC and CCCC, we assume the presence of minor gaps for PRPC and CCCC. As stated in Goto *et al.* (2019), such gaps

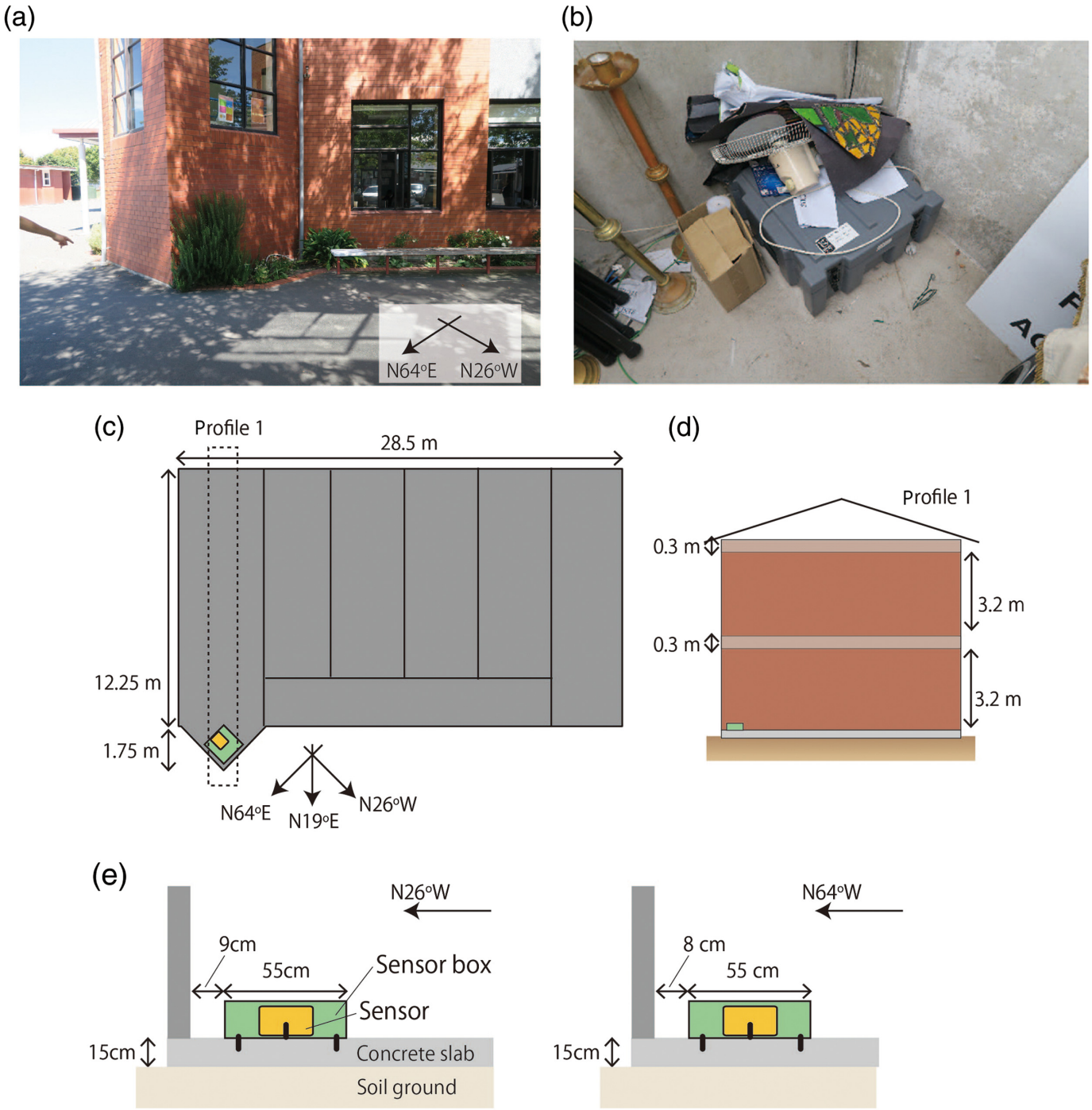

Figure 5. Installation conditions at CCCC. Photo of (a) exterior view and (b) sensor box. (c) Plan view and (d,e) cross-section views. The color version of this figure is available only in the electronic edition.

may have been created by soil erosion or differential settlement of the soil. As we do not have any constraints on the width and length of a gap at each station, we vary these parameters and discuss the dependence of these parameters on the resulting motions as presented in the Appendix.

The actual slab structures are also represented by the equivalent 2D models. The slab is discretized into 0.25 m width of finite elements assuming a Euler–Bernoulli beam with three degrees of freedom per node: horizontal, vertical translation, and rotational components (Reissner, 1972; Scott, 1981). The Young's modulus and density are 30 GPa and 2400 kg/m^3, respectively, representing the physical properties of standard concrete. The reaction force from the soil is modeled using Winkler springs, a system of identical but mutually independent, linear elastic springs. The vertical springs are able to separate when the initial weight is released. The horizontal springs represent the frictional force, with the maximum value

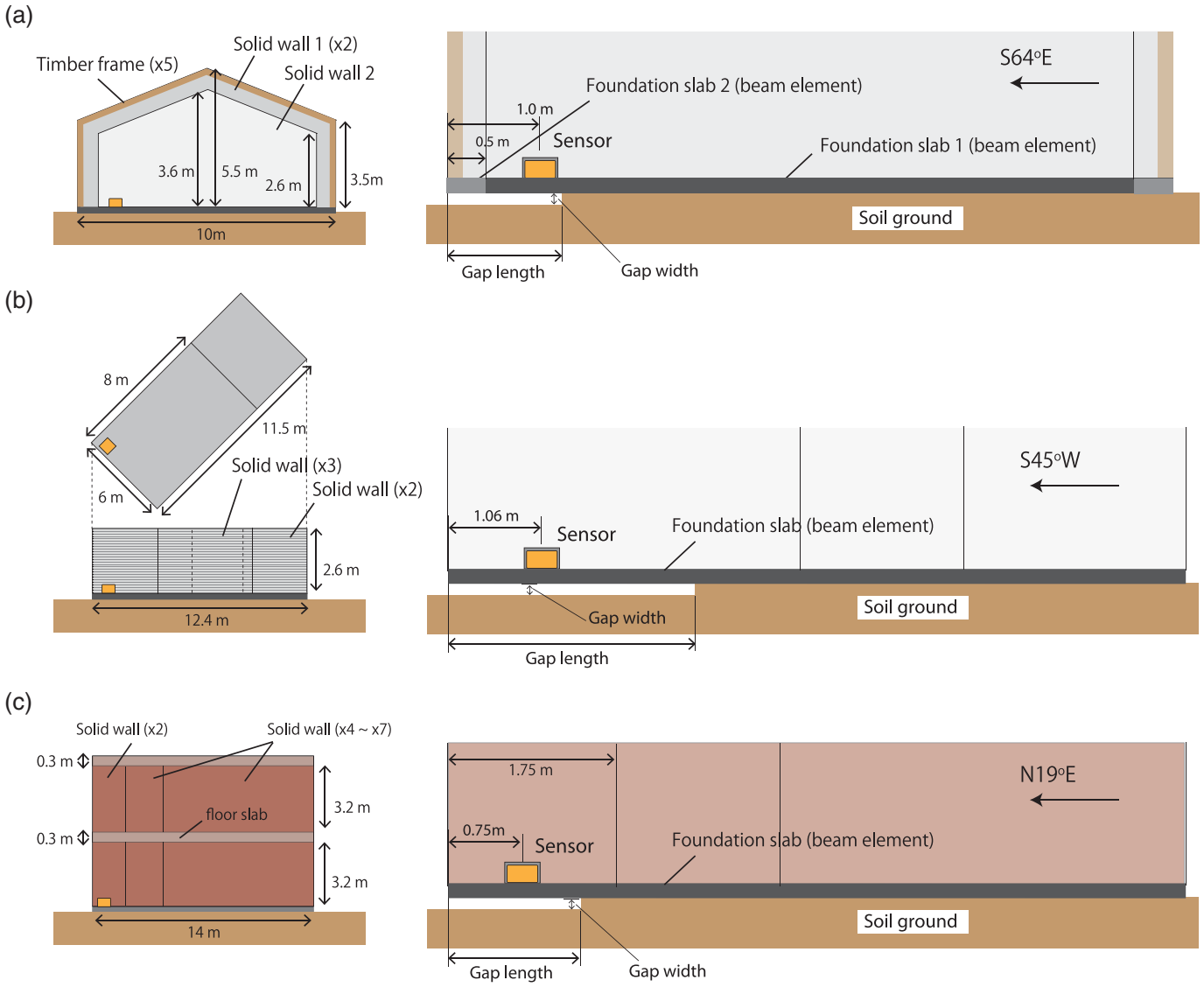

Figure 6. Numerical models of structure and underlying soil ground for (a) HVSC, (b) PRPC, and (c) CCCC. The color version of this figure is available only in the electronic edition.

constrained by the static friction that is proportional to the normal force. When the horizontal force exceeds the maximum static friction, horizontal sliding occurs. These springs are connected to all of the nodes of the slab elements.

The vertical and horizontal spring coefficients are evaluated with the equation by Gazetas (1991). The density and Poisson's ratio of the soil ground are set to 1750 kg/m^3 and 0.30, respectively. We check the *S*-wave velocity and friction coefficient values from parameter surveys as shown in the Appendix. Self-gravity deformation is calculated prior to the ground-motion excitation. This process sets the initial deformation of the elastic slab as well as the initial weights acting on each spring before the ground-motion excitations.

Low-pass-filtered accelerations for both the horizontal and vertical components are assumed as input ground motions following the approach by Goto *et al.* (2019). Figure 7a shows the power spectrum of the vertical accelerations during the mainshock of the Christchurch earthquake. A few peaks appear in the higher-frequency range (>13 Hz) and are separated from the main peaks in the lower-frequency range, especially for HVSC and PRPC (Fig. 7). Based on an analogy from nonlinear acoustic contacts (e.g., Solodov *et al.*, 2002; Biwa *et al.*, 2004) in a field of nondestructive tests, the higher-frequency components are assumed to be induced due to the contacts. We select 15 Hz and 13 Hz as the cutoff frequency for HVSC and PRPC records, respectively.

Figure 7b compares the low-pass-filtered waveforms with the original records. The filtered waveforms are symmetric; however, the dominant phases are retained, as shown in the raw data from HVSC and PRPC. This confirms that frequencies above the cutoff values lead to the waveform asymmetry. The induced high-frequency components are not clear for CCCC as shown in Figure 7a. Hence, several cutoff frequencies are tested and

TABLE 1
Dimension and Physical Parameters of Upper Structure at HVSC Station

Foundation slab	Young's modulus	30 GPa
	Density	2400 kg/m^3
	Height	0.228 m (0–0.5 m, 9.5–10 m)
		0.270 m (0.5–9.5 m)
	Thickness	33.3 m
	Element type	Euler–Bernoulli beam
	Element length	0.25 m
Timber frame	Young's modulus	10 GPa
	Density	700 kg/m^3
	Width	0.15 m
	Thickness	0.15 m
	Element type	Euler–Bernoulli beam
	Element length	3.5 m, 5.39 m
Solid wall 1	Young's modulus	10 GPa
	Density	700 kg/m^3
	Poisson's ratio	0.40
	Thickness	0.08 m
	Stress state	Plane stress
	Element type	4-node isoparametric element
	Element length	0.25 m
	Element height	0.65–0.90 m
Solid wall 2	Young's modulus	10 GPa
	Density	700 kg/m^3
	Poisson's ratio	0.40
	Thickness	0.08 m
	Stress state	Plane stress
	Element type	4-node isoparametric element
	Element length	0.25 m
	Element height	0.875–1.375 m

TABLE 2
Dimension and Physical Parameters of Upper Structure at PRPC Station

Foundation slab	Young's modulus	30 GPa
	Density	2400 kg/m^3
	Height	0.13 m
	Thickness	0–8.49 m
	Element type	Euler–Bernoulli beam
	Element length	0.177 m
Solid wall	Young's modulus	20 GPa
	Density	2000kg/m^3
	Poisson's ratio	0.20
	Thickness	0.283 m
	Stress state	Plane stress
	Element type	4-node isoparametric element
	Element length	0.177 m
	Element height	0.65 m

TABLE 3
Dimension and Physical Parameters of Upper Structure at CCCC Station

Foundation slab	Young's modulus	30 GPa
	Density	2400 kg/m^3
	Height	0.15 m
	Thickness	0–3.5 m (0–1.75 m)
		28.5 m (1.75–14 m)
	Element type	Euler–Bernoulli beam
	Element length	0.25 m
Floor slab	Young's modulus	20 GPa
	Density	2000 kg/m^3
	Poisson's ratio	0.20
	Height	0.30 m
	Thickness	28.5 m
	Stress state	Plane stress
	Element type	4-node isoparametric element
	Element length	0.25 m
	Element height	0.30 m
Solid wall	Young's modulus	20 GPa
	Density	2000 kg/m^3
	Poisson's ratio	0.20
	Height	3.2 m
	Thickness	0.212 m
	Stress state	Plane stress
	Element type	4-node isoparametric element
	Element length	0.25 m
	Element height	0.80 m

compared with the original records. We then assume 15 Hz as the cutoff frequency for station CCCC (Fig. 7b).

We selected parameter values of gap length, gap width, *S*-wave velocity, and the friction coefficient from the simulation results of the parametric study (see the Appendix). At HVSC, the gap length, gap width, *S*-wave velocity, and friction coefficient are set to (1.0 m, 0.6 mm, 300 m/s, and 0.75), respectively. At PRPC and CCCC, they are (4.95 m, 1.2 mm, 350 m/s, and 0.5) and (1.75 m, 0.6 mm, 350 m/s, and 0.5), respectively. Figure 8 shows the simulated responses against the original waveforms for both the mainshock and aftershock using the selected model parameters. Results show that simulations for all of these stations reproduce the observed asymmetric phases quite well in the vertical components. The positive accelerations for the M_w 6.2 mainshock at HVSC exceed 2*g*, whereas the negative accelerations are confined around 1*g*, consistent with the observation. Slight asymmetry in the aftershock records is also reproduced with the same station response as in the mainshock.

Observed vertical accelerations for CCCC are well reproduced by the numerical model, whereas the vertical asymmetry is not well simulated in terms of *Fp* (Fig. A1). As discussed in Figure 2, CCCC may be contaminated by soil–structure collisions. This suggests that the simulation model at CCCC is likely too simple to explain the causes of AsVAs. More precise investigation is needed to clear the source of AsVAs for the station CCCC.

Figure 9a,b shows the comparison of power spectra of vertical accelerations for the mainshock. Although frequency components higher than 15 Hz at HVSC and 13 Hz at PRPC are not included in the input motions, they are well

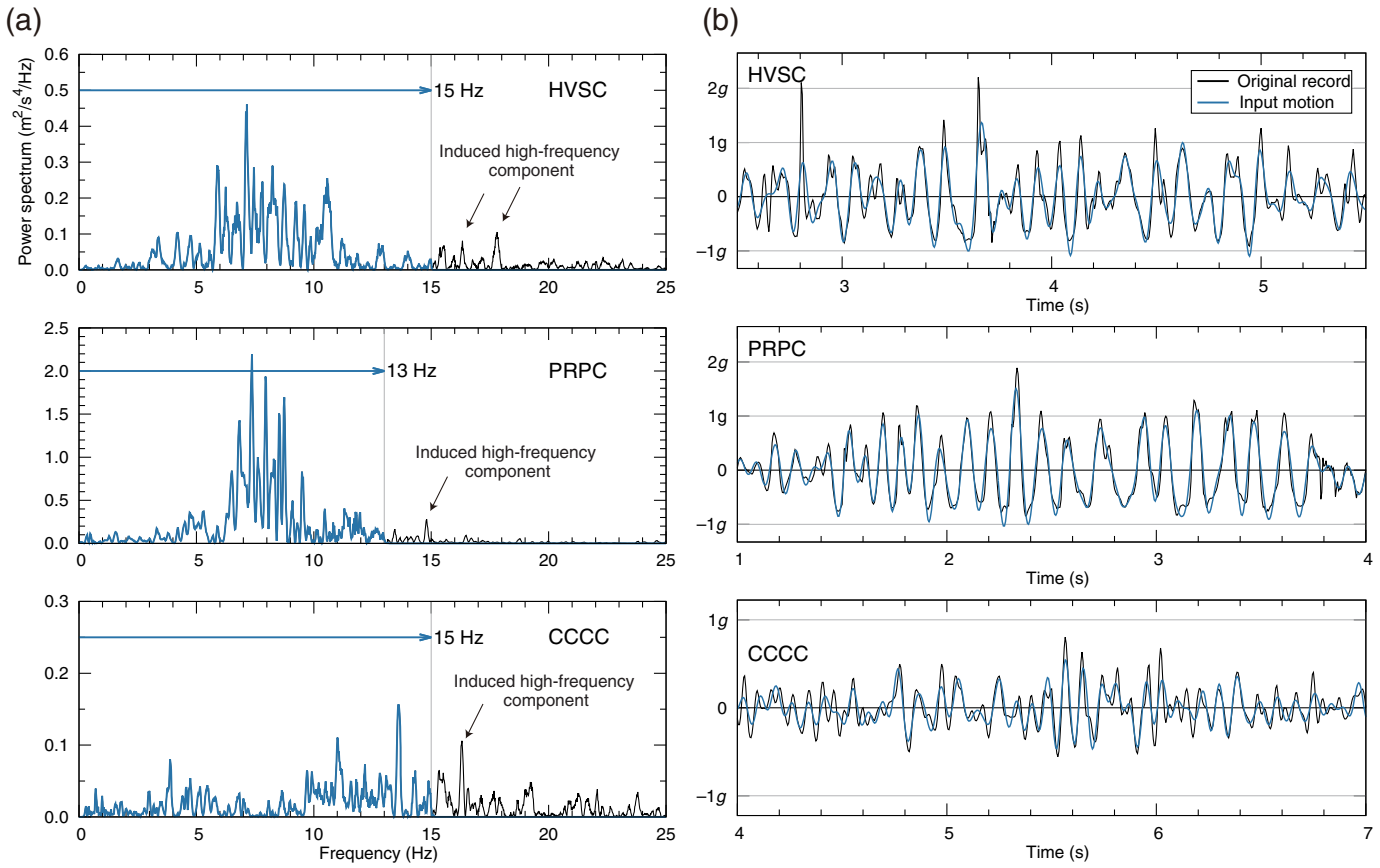

Figure 7. (a) Power spectrum of vertical accelerations during the 2011 M_w 6.2 Christchurch earthquake at HVSC, PRPC, and CCCC. (b) Comparison between the original records and low-pass-filtered vertical accelerations (input motions). From the analysis of power spectrum, the cutoff frequencies are chosen to be 15, 13, and 15 Hz for HVSC, PRPC, and CCCC, respectively. The color version of this figure is available only in the electronic edition.

reproduced by the simulation results. If the system is linear (i.e., not accounting for the effects of soil–structure collisions), the higher frequencies cannot be excited. Figure 9c shows a zoom-in of vertical accelerations indicated in Figure 8a. The observed phases are well explained by the simulation results. Positive accelerations are enhanced due to the impact of the slab on the underlying soil (Fig. 9d). At negative acceleration peaks, the slab beneath the sensor detaches from the soil, which is a key characteristic of the interaction. Overall, these numerical models that incorporate soil–structure collisions are able to explain the observed AsVA records.

These results suggest that the actual ground accelerations during the 2011 Christchurch earthquake are overestimated at HVSC and PRPC. The symmetric input motions assumed in the numerical models (Fig. 7) imply that the actual peak vertical accelerations are 1.37*g* and 1.51*g* at HVSC and PRPC, respectively, during the mainshock, instead of the original records of 2.20*g* and 1.89*g*.

DISCUSSIONS

The results of numerical simulations suggest that the AsVAs recorded during the mainshock and aftershock of the 2011 Christchurch earthquake can be explained by soil–structure collisions, which is similar to the mechanism previously proposed to explain large AsVAs at WTMC during the 2016 Kaikōura earthquake (Goto *et al.*, 2019). The generation mechanism of large AsVAs in the present models involves the collisions of the base foundation onto the underlying soil via both the flapping effect (Goto *et al.*, 2019) and rocking (Ohmachi *et al.*, 2011). Large peak accelerations during the 2011 M_w 6.2 earthquake reported previously were likely induced by the dynamic interactions of a building structure and underlying ground, which do not reflect actual ground motions. Previous studies on horizontal components of the HVSC records by Jeong and Bradley (2017a,b) revealed that the 1D nonlinear site response dominates in the lower-frequency (<3 Hz) range and Rayleigh waves induced by the basin edge contribute to the higher-frequency (>3 Hz) excitations. However, the extent at which the Rayleigh waves excite the high-frequency (>15 Hz), AsVAs at HVSC is not clear from their studies. Even if 1D/2D site amplifications are prevalent at HVSC, soil–structure collisions would still be an important factor that leads to large AsVAs.

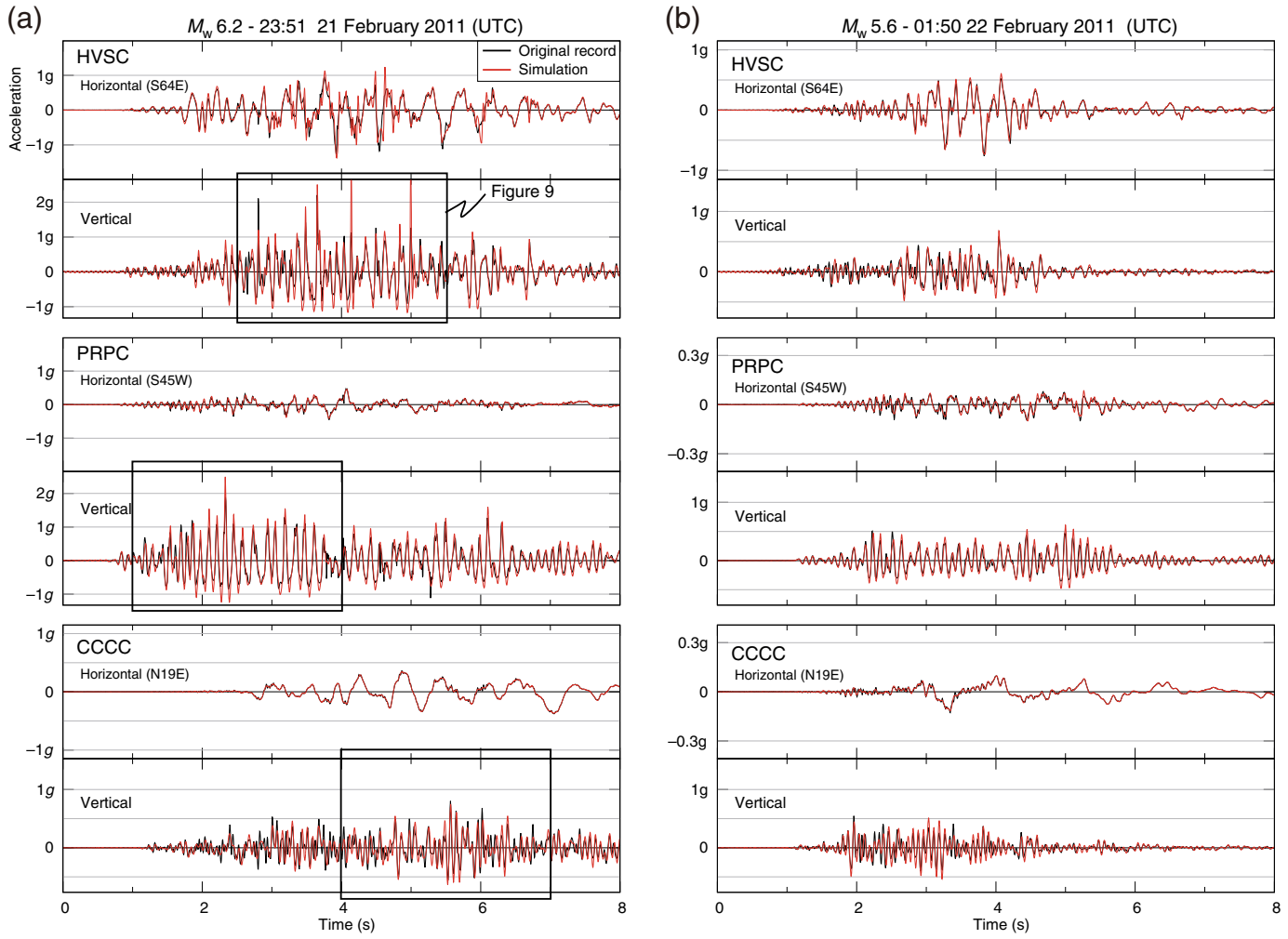

Figure 8. Simulated horizontal and vertical accelerations at HVSC, PRPC, and CCCC for (a) the M_w 6.2 mainshock and (b) M_w 5.6 aftershock of the 2011 Christchurch earthquake. Solid boxes indicate the focus sections shown in Figure 9. Low-pass-filtered acceleration records for both the horizontal and vertical components shown in Figure 7 are used as input ground motions to each simulation. The color version of this figure is available only in the electronic edition.

The filtered waveforms (i.e., input ground motions shown in Fig. 7) still show some minor levels of waveform asymmetry. Also, weak ground motions analyzed in this study indicate both positive and negative asymmetries (Fig. 2). In general, waveform asymmetry could be caused by soil–structure collisions as well as source and site effects (e.g., the presence of a hill). We do not assert that all levels of asymmetry are attributed to soil–structure collisions only. Our results highlight how soil–structure collisions can significantly enhance the asymmetry of vertical accelerations during large, input ground motions.

Installing seismic sensors outside of building structures (i.e., in a free field) may help mitigate soil–structure collisions that can contaminate the actual ground motions. The presence of a foundation slab can cause soil–structure interactions that can reduce incoherent high-frequency signals due to spatial averaging (e.g., Hoshiya and Ishii, 1983; Luco and Wong, 1986; Kim and Stewart, 2003). However, in an urban area, finding such free-field sites may be challenging for a number of practical reasons. As a result, seismic sensors are often installed on the floor of a shed or building. In this case, one needs to mitigate the soil–structure interaction to properly capture the actual ground motions.

Installation conditions for CBGS and SHLC may offer a good example for minimizing the effect of soil–structure collisions. As shown in Figures 1 and 2, CBGS and SHLC recorded no significant AsVAs for all earthquakes analyzed in this study. Figure 10 shows the installation conditions at these stations. CBGS is installed in the Christchurch Botanic Garden, specifically within the former gravity observatory with floor dimensions of 6.1 m by 4.3 m. The sensor was placed along one edge of this room, in the middle (Fig. 10a). SHLC is installed in a single-story library building located in Shirley (Fig. 10b). The sensor is situated in a small room far from the corner of a foundation slab. The sensor locations at CBGS and SHLC suggest that placing seismic sensors away from the corner of a

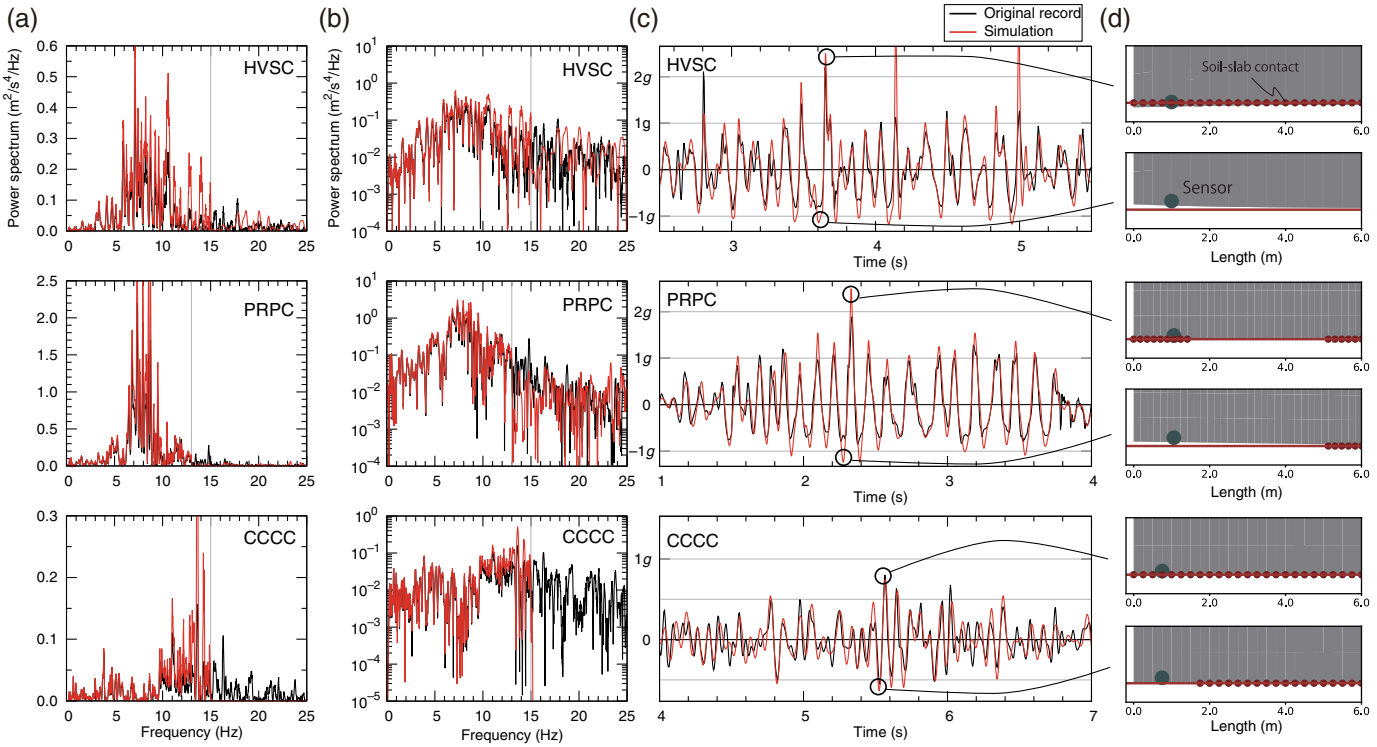

Figure 9. (a) Power spectra of vertical accelerations compared between the observed and simulated ones at HVSC, PRPC, and CCCC for the M_W 6.2 mainshock. (b) Logarithmic scale of the power spectra. (c) Focus sections of vertical accelerations indicated in Figure 8. (d) Deformation diagrams at negative and positive acceleration peaks indicated in (c). The solid green circle indicates the sensor location. The brown circles represent soil–slab contacts. The color version of this figure is available only in the electronic edition.

Figure 10. Installation conditions at (a) CBGS and (b) SHLC. Sensor positions are indicated. The color version of this figure is available only in the electronic edition.

foundation slab may mitigate soil–structure collisions and, hence, the artificial AsVAs.

We test this hypothesis using a numerical simulation at PRPC. A hypothetical new sensor (sensor 2) is placed near the center of the foundation slab, and the response is compared with that of the sensor located at the original position (sensor 1; Fig. 11a). The same model parameters are used, as discussed in previous simulations for the 2011 Christchurch earthquake

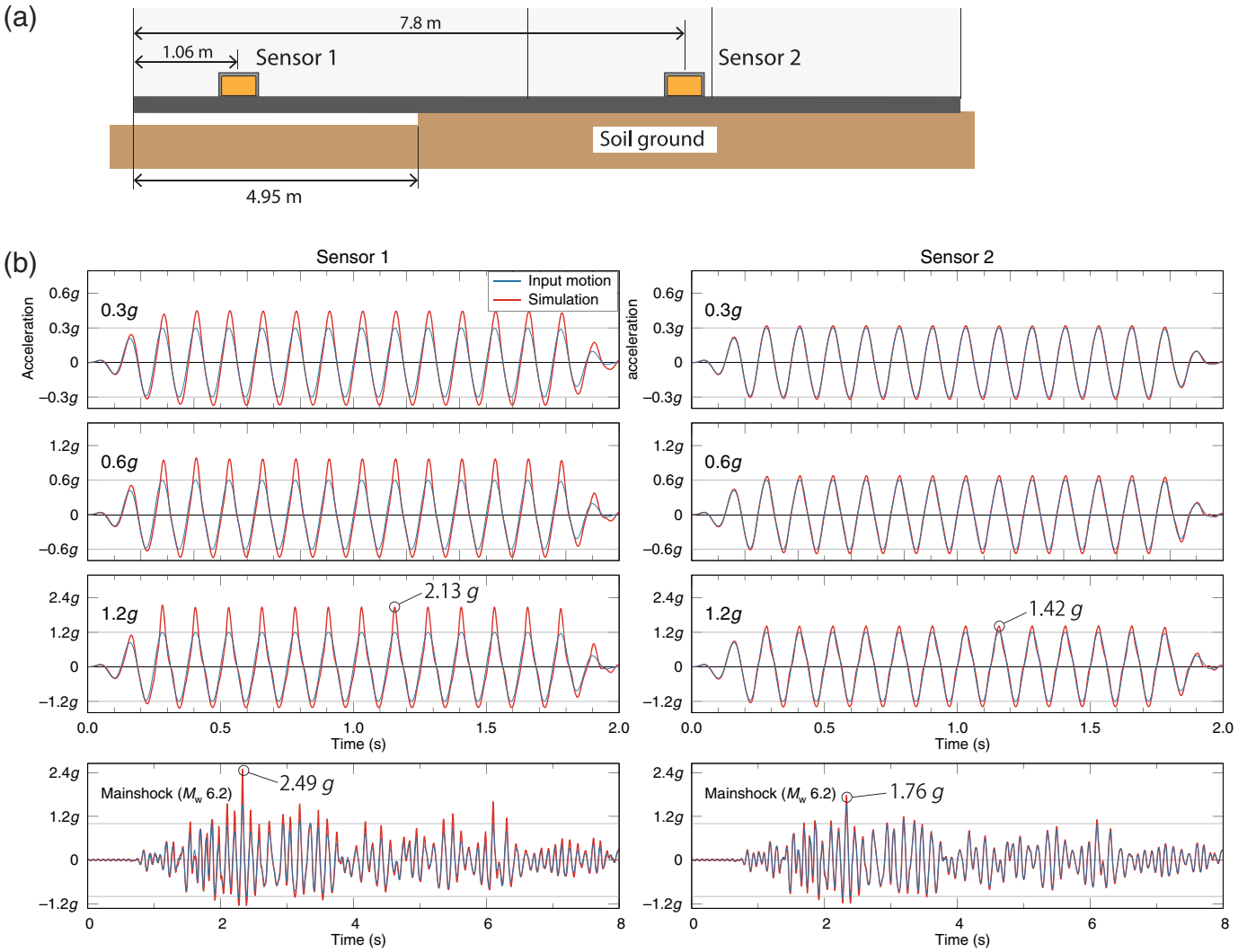

(Fig. 6b). Sinusoidal excitations with variable amplitudes of 0.3*g*, 0.6*g*, and 1.2*g* are used as inputs in the model. The responses at the location of sensors 1 and 2 are calculated, and the results are shown in Figure 11b. The simulated vertical response at sensor 1 shows clear AsVAs as the amplitude of the input sinusoidal motions increases. In contrast, the response at sensor 2 is almost identical to the input motions even when the input motions are large (e.g., 1.2*g*). The mainshock of the 2011 M_w 6.2 Christchurch earthquake is also simulated using both sensors 1 and 2. As shown in Figure 11b, the AsVA response observed at sensor 1 does not appear at sensor 2. The positive peak decreases to 1.76*g* compared with the original value of 2.49*g*. These results suggest that sensors located near the corner of a foundation slab are more prone to soil–structure collisions, whereas sensors at the center of a slab can generate records showing the actual ground motions. We further test the sensitivity of this conclusion to different station conditions (such as the one shown in Fig. 12). These additional tests confirm that the elastic flapping effect can be mitigated by placing sensors away from the corner of a foundation slab.

Figure 11. Simulated responses of PRPC under sinusoidal input ground motions with a variety of amplitudes and the mainshock of the 2011 M_w 6.2 Christchurch earthquake. (a) Description of model 1 and sensor locations. (b) Vertical responses (red) under sinusoidal excitations and the M_w 6.2 mainshock of the 2011 Christchurch earthquake (blue). Sensor 2 is less prone to the elastic flapping effect than sensor 1. The color version of this figure is available only in the electronic edition.

These simulation results (Figs. 11 and 12) suggest that the sensor should be placed closer to the middle of a foundation slab and away from the corner. To further validate this inference, we produce histograms of *Fs*, *Fp*, and *Fh* using models 1 (PRPC model) and 2 and input motions derived from all 387 earthquake records. Figure 13 shows the histograms of *Fs*, *Fp*, and *Fh*, estimated from the simulated responses at sensor 1 and sensor 2 using models 1 (PRPC model) and 2. The histograms show a shift in the positive direction for larger peak accelerations at sensor 1 for both models 1 and 2. The positive shift is less clear at sensor 2 (i.e., the lack of soil–structure collisions) even under large input motions. This comparison confirms that sensors situated near the center of a foundation slab foundation

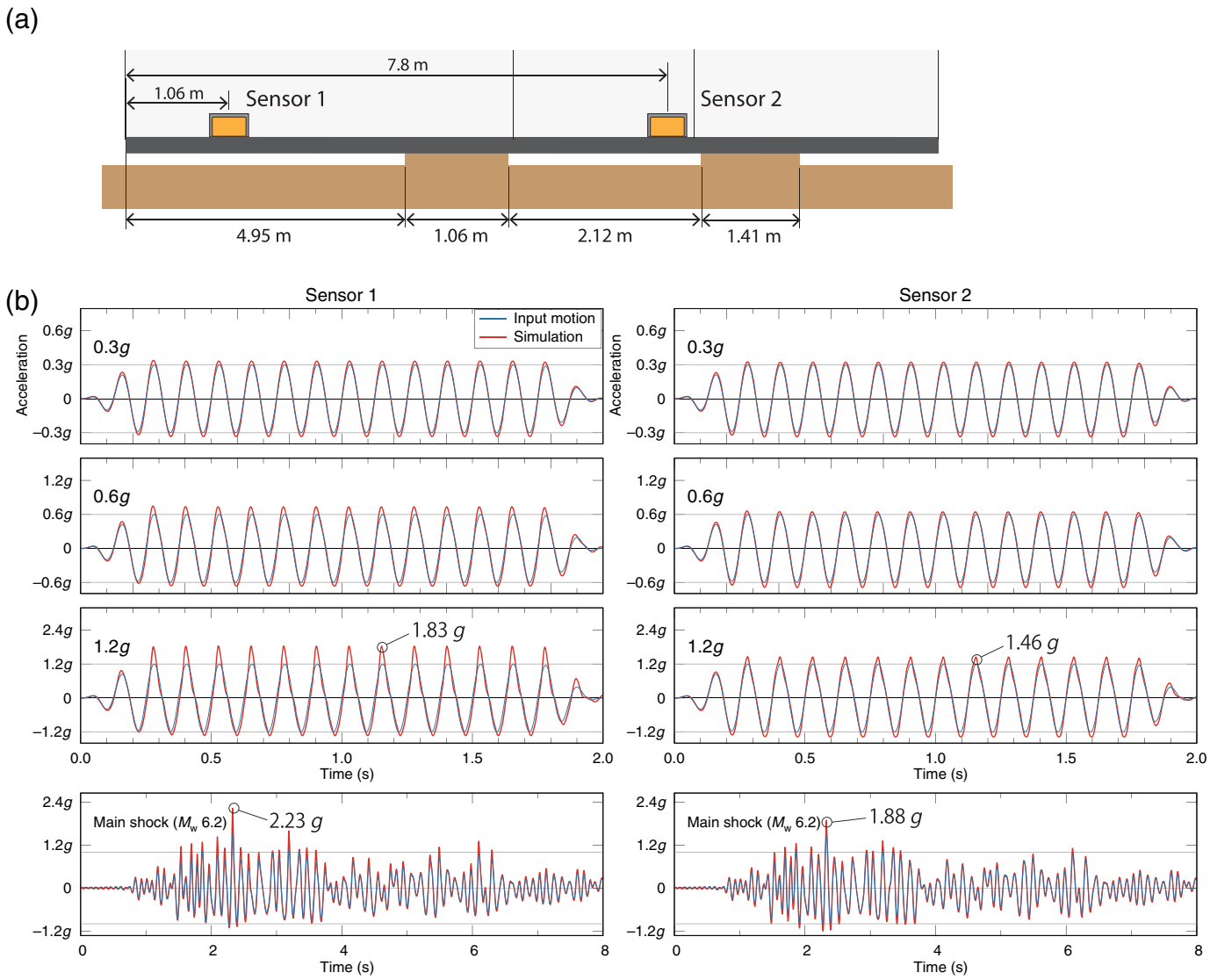

Figure 12. Simulated responses at PRPC under sinusoidal input ground motions with a variety of amplitudes and the mainshock of the 2011 M_w 6.2 Christchurch earthquake. (a) Description of model 2 and sensor locations. (b) Vertical responses (red) under sinusoidal excitations and the M_w 6.2 mainshock of the 2011 Christchurch earthquake (blue). Sensor 2 is less prone to the elastic flapping effect than sensor 1. The color version of this figure is available only in the electronic edition.

are less prone to soil–structure collisions. We emphasize again that this mitigation strategy caters to situations in which the sensor needs to be installed in a shed or building.

Two important simplifications are made in our model. First, we assume that soil–slab interactions can be represented by linear elastic springs without considering soil nonlinearity. A previous study (Goto *et al.*, 2019) examined the effect of an elasto-plastic spring in a similar problem and showed that, although the peak amplitude can be diminished, nonlinear soil response does not affect the essential behavior of the model. Second, models considered in this study are limited in 2D space, and we assume that both the slab and gap between the concrete foundation and underlying soil continue infinitely in the third (antiplane) direction (Fig. 6). Hence probable 3D effects are not fully accounted for in this model. This means that other possible mechanisms that might explain the observed large AsVAs cannot be ruled out at this stage. We consider physical processes of a simplified, local system response that mimics the actual station conditions. To robustly validate the occurrence of soil–structure collisions, realistic 3D models with 3D gap distributions would be required, which remains a subject of future work.

CONCLUSIONS

We have investigated the origin of large, AsVAs recorded at seismic stations HVSC, PRPC, and CCCC during the 2011 Christchurch earthquake sequence. Three metrics, namely *Fs*, *Fp*, and *Fh*, have been proposed to quantify the degree of waveform asymmetry. The histograms of *Fs*, *Fp*, and *Fh* compiling all of the available records at PRPC and CCCC show a clear

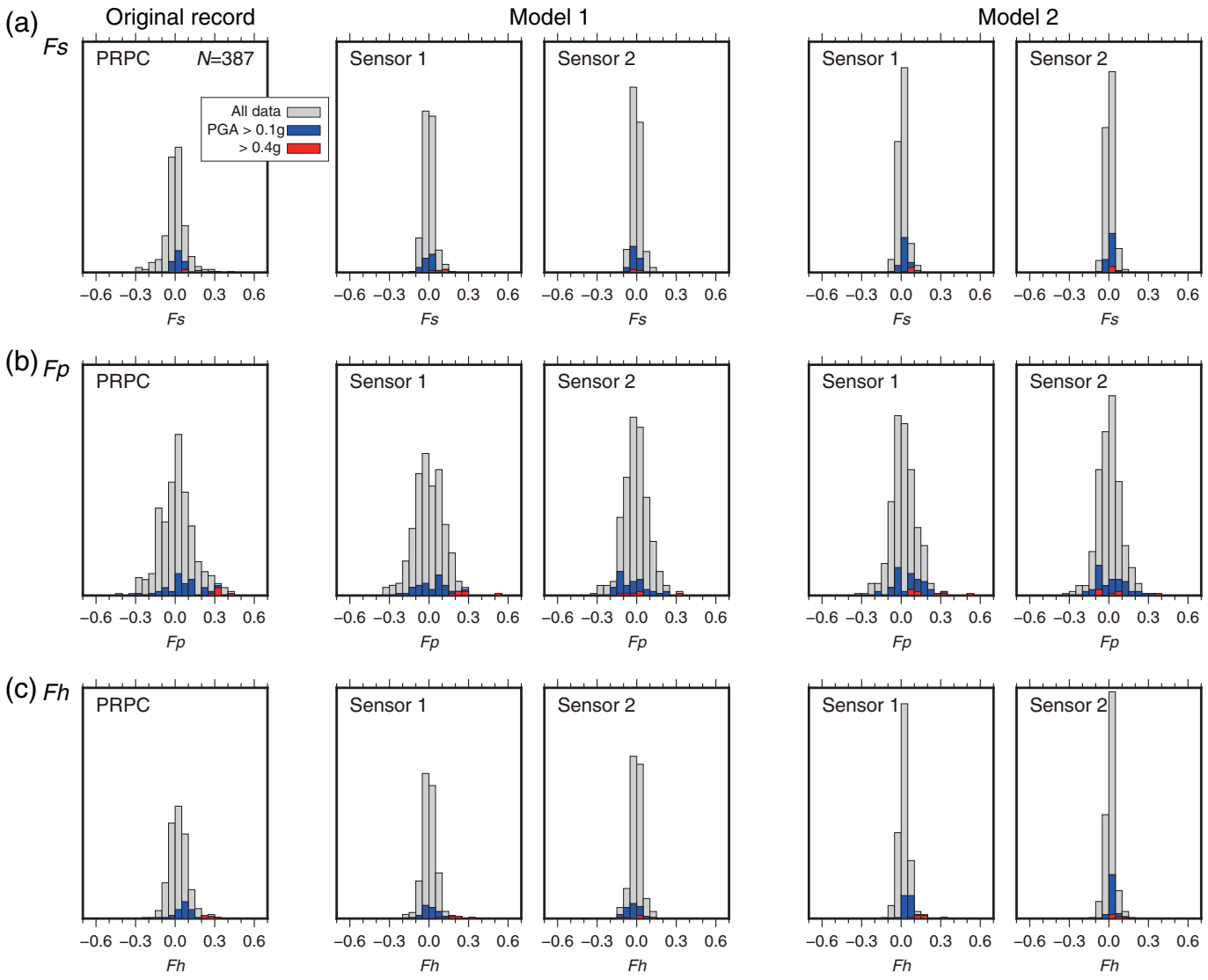

Figure 13. Histograms showing the degree of asymmetry in the vertical-component waveform records at PRPC and simulated waveforms using models 1 and 2 shown in Figures 11 and 12, respectively. Three metrics (a) *Fs*, (b) *Fp*, and (c) *Fh* are defined in the QUANTIFICATION OF AsVAs RECORDS section. Gray background represents all waveform data, whereas blue and red colored histograms are for the waveform data exceeding a PGA of 0.1*g* and 0.4*g*, respectively. For both models 1 and 2, large AsVAs due to the flapping effect are significantly reduced at sensor 2, which is located closer to the center of the foundation slab. The color version of this figure is available only in the electronic edition.

shift in the positive direction (i.e., more asymmetry) for larger accelerations. This suggests that the waveform records at PRPC and CCCC may be affected by the local system response induced by soil–structure collisions, a type of nonlinear, soil–structure interaction that involves the collisions of a base foundation onto the underlying soil (Ohmachi *et al.*, 2011; Goto *et al.*, 2019). The histograms for HVSC did not clearly show the evidence of AsVAs under the weaker motions, but the larger acceleration records exceeding 0.4*g* indicate the existence of the AsVAs.

Overall, these metrics and corresponding histograms aid in detecting and identifying strong-motion stations that may be prone to soil–structure collisions when acceleration records yield PGA $>$ 0.4*g*. However, in practice, many strong-motion stations have not yet experienced such large accelerations. Once large accelerations are generated by nearby earthquake sequences in the future, these metrics would be useful not only in identifying the occurrence of AsVAs but also in quantitatively assessing whether the observed AsVAs represent the actual ground shaking or are contaminated by soil–structure collisions.

We have conducted numerical simulations of station responses and successfully reproduced the large AsVAs observed during the mainshock and aftershock of the 2011 M_w 6.2 Christchurch earthquake. The model parameters at each station are largely constrained by our site investigation, and we have explored the sensitivity of the results to unconstrained parameters. We have found that the numerical simulations reproduce observed waveforms for both the mainshock and M_w 5.6 aftershock of the 2011 M_w 6.2 Christchurch

earthquake for all of the stations with and without AsVAs. Our results suggest that large, AsVAs can be explained by soil–structure collisions and that the actual ground accelerations during the 2011 Christchurch earthquake are overestimated at several stations. The estimated PGA at station HVSC is 1.37*g* as opposed to the recorded value of 2.2*g*.

The sensors at HVSC, PRPC, and CCCC are located at the corner of foundation slabs in building structures. In contrast, the sensors at CBGS and SHLC that do not show AsVAs are located away from the corner of foundation slabs. We have confirmed from additional numerical simulations that the local system response due to soil–structure collisions is enhanced near the corner of the foundation slab. Our results also suggest that artificial recording of large AsVAs due to soil–structure collisions can be mitigated if the seismic sensor is placed closer to the center of a foundation slab. In the future, this simple mitigation strategy can be tested via the deployment of two identical sensors placed at different locations of a foundation slab.

DATA AND RESOURCES

Acceleration records at seismic stations WTMC, HVSC, PRPC, CCCC, CBGS, and SHLC are available from the Global Positioning System (GPS) Earth Observation Network System (GeoNet) Strong Motion Data Products, available at https://www.geonet.org.nz/data/types/strong_motion (last accessed October 2020), and accessible through International Federation of Digital Seismograph Networks (FDSN) webservice, available at https://www.geonet.org.nz/data/tools/FDSN (last accessed October 2020).

ACKNOWLEDGMENTS

The authors thank Associate Editor Luis A. Dalguer, John Anderson, and Hamish Avery for their valuable feedback and comments. This work is supported by the Program for Fostering Globally Talented Researchers by Japan Society for the Promotion of Science (G2901) and public funding from the Government of New Zealand.

REFERENCES

Anderson, J. G. (2010). Source and site characteristics of earthquakes that have caused exceptional ground accelerations and velocities, *Bull. Seismol. Soc. Am.* **100,** 1–36.

Anderson, J. G., I. Tibuleac, A. Anooshehpoor, G. Biasi, K. Smith, and D. von Seggern (2009). Exceptional ground motions recorded during the 26 April 2008 M_w 5.0 earthquake in Mogul, Nevada, *Bull. Seismol. Soc. Am.* **99,** 3475–3486.

Aoi, S., T. Kunugi, and H. Fujiwara (2008). Trampoline effect in extreme ground motion, *Science* **322,** 727–730.

Bielak, J. (1974). Dynamic behavior of structures with embedded foundations, *Earthq. Eng. Struct. Dynam.* **3,** 259–274.

Biwa, S., S. Nakajima, and N. Ohno (2004). On the acoustic nonlinearity of solid-solid contact with pressure-dependent interface stiffness, *J. Appl. Mech.* **71,** 508–515.

Dhakal, Y. P., T. Kunugi, T. Kimura, W. Suzuki, and S. Aoi (2019). Peak ground motions and characteristics of nonlinear site response during the 2018 M_w 6.6 Hokkaido eastern Iburi earthquake, *Earth Planets Space* **71,** 56.

Fry, B., R. Benites, and A. Kaiser (2011). The character of accelerations in the M_w 6.2 Christchurch earthquake, *Seismol. Res. Lett.* **82,** 846–852.

Gazetas, G. (1991) Formulas and charts for impedances of surface and embedded foundations, *J. Geotech. Eng.* **117,** 1363–1381.

Goto, H., and H. Morikawa (2012). Ground motion characteristics during the 2011 off the Pacific Coast of Tohoku earthquake, *Soils Found.* **52,** 769–779.

Goto, H., Y. Kaneko, J. Young, H. Avery, and L. Damiano (2019). Extreme accelerations during earthquakes caused by elastic flapping effect, *Sci. Rep.* **9,** 1117.

Honda, R., S. Aoi, N. Morikawa, H. Sekiguchi, T. Kunugi, and H. Fujiwara (2005). Ground motion and rupture process of the 2004 Mid Niigata Prefecture earthquake obtained from strong motion data of K-NET and KiK-net, *Earth Planets Space* **57,** 527–532.

Hoshiya, M., and M. Ishii (1983). Evaluation of kinematic interaction of soil-foundation systems by a stochastic model, *Int. J. Soil. Dynam. Earthq. Eng.* **2,** 128–134.

Jennings, P. C., and J. Bielak (1973). Dynamics of building-soil interaction, *Bull. Seismol. Soc. Am.* **63,** 9–48.

Jeong, S., and B. A. Bradley (2017a). Amplification of strong ground motions at Heathcote valley during the 2010-2011 Canterbury earthquakes: Observation and 1D site response analysis, *Soil Dynam. Earthq. Eng.* **100,** 345–356.

Jeong, S., and B. A. Bradley (2017b). Amplification of strong ground motions at Heathcote valley during the 2010-2011 Canterbury earthquakes: The role of 2D nonlinear site response, *Bull. Seismol. Soc. Am.* **107,** 2117–2130.

Kausel, E. (2010). Early history of soil-structure interaction, *Soil Dynam. Earthq. Eng.* **30,** 822–832.

Kim, S., and J. P. Stewart (2003). Kinematic soil-structure interaction from strong motion recordings, *J. Geotech. Geoenviron. Eng.* **129,** 323–335.

Luco, J. E., and H. L. Wong (1986). Response of a rigid foundation to a spatially random ground motion, *Earthq. Eng. Struct. Dynam.* **14,** 891–908.

Maeda, T., and T. Sasatani (2009). Strong ground motions from an M_j 6.1 inland crustal earthquake in Hokkaido, Japan: The 2004 Rumoi earthquake, *Earth Planets Space* **61,** 689–701.

Ohmachi, T., S. Inoue, T. Mizuno, and M. Yamada (2011). Estimated cause of extreme acceleration records at the KiK-net IWTH25 station during the 2008 Iwate-Miyagi Nairiku earthquake, Japan, *J. JAEE* **11,** 32–47 (in Japanese with English abstract).

Porcella, R. L., and R. B. Matthieson (1979). Preliminary summary of the U.S. Geological Survey strong motion records from Oct. 15, 1979 Imperial Valley Earthquake, *U.S. Geol. Surv. Open-File Rept. No. 79-1654.*

Reissner, E. (1972). On one-dimensional finite-strain beam theory: The plane problem, *J. Appl. Math. Phys.* **23,** 795–804.

Robertson, I. A. (1966). Forced vertical vibration of a rigid circular disc on a semi-infinite elastic solid, *Math. Proc. Camb. Philos. Soc.* **62,** 547–553.

Scott, R. F. (1981). *Foundation Analysis*, Prentice-Hall, Englewood Cliffs, New Jersey.

Shakal, A., M. Huang, R. Darragh, T. Cao, R. Sherburne, P. Malhotra, C. Cramer, R. Sydnor, V. Graizer, G. Maldonado, *et al.* (1994). CSMIP strong-motion records from the Northridge, California earthquake of January 17, 1994, *Report No. OSMS 94-07.*

Solodov, I. Y., N. Krhohn, and G. Busse (2002). CAN: An example of nonclassical acoustic nonlinearity in solids, *Ultrasonics* **40,** 621–625.

Sotiriadis, D., N. Klimis, B. Margaris, and A. Sextos (2019). Influence of structure-foundation-soil interaction on ground motions recorded within buildings, *Bull. Earthq. Eng.* **17,** 5867–5895.

U.S. Geological Survey (USGS) (1976). *Strong-motion record from the May 17, 1976 Gazli, U.S.S.R. Earthquake*, *Seismic Engineering Program Report*, October-December 1976, Circular 736-D.

Veletsos, A. S., and J. W. Meek (1974). Dynamic behavior of building-foundation systems, *Earthq. Eng. Struct. Dynam.* **3,** 121–138.

APPENDIX

Model parameter sensitivity

Because the gap width and length are not constrained by our site investigation, several sets of the parameter values are examined. The gap length is defined herein as the distance from the edge (i.e., 0 m represents no gaps and in full contact with the soil ground). Figure A1 shows the simulation results quantified using *Fp* (equation 2) and the peak accelerations for both the mainshock and the aftershock. As the gap length increases, asymmetric vertical acceleration (AsVA) tends to be enhanced under the large input motion (e.g., $>1g$ for the mainshock), whereas the local maximum for AsVA exists at a certain gap length under weaker motions especially. This critical gap length in which the local maximum for AsVA exists depends on the gap width. Hence these parameters are relatively tightly constrained at least within our models. The model parameters, as indicated by the black square boxes in Figure A1, yield the best representation of the original records for both the mainshock and aftershock.

We further examine sensitivities to other unconstrainted model parameters related to the soil–structure interface. The *S*-wave velocity and friction coefficient examined are 200–400 m/s and 0.25–1.0, respectively. Parameters such as gap width and length (depicted in Fig. A1) are held constant, and the results are quantified in terms of *Fp* and vertical and horizontal peak accelerations (Fig. A2). We find that a change in the friction coefficient affects only the horizontal components of peak ground accelerations at HVSC and hence does not influence AsVA. In contrast, the change in *S*-wave velocity influences the magnitude of *Fp* and vertical accelerations.

Manuscript received 22 October 2020
Published online 5 January 2021

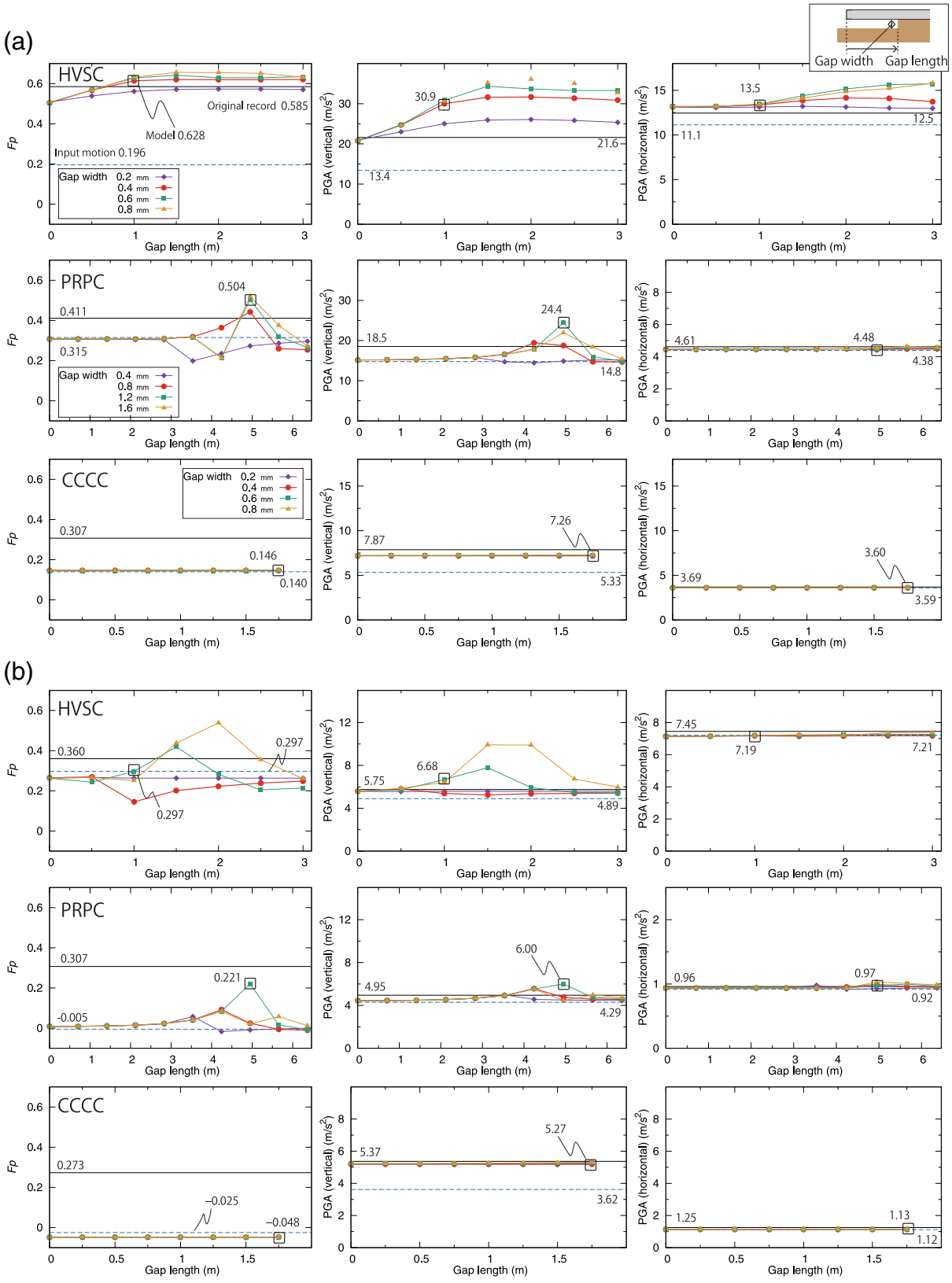

Figure A1. Dependence of the gap width and length of soil underneath the concrete slab (inset figure) on the resulting waveform asymmetry. A simulated AsVA is characterized by *Fp* and peak accelerations for (a) the 2011 M_w 6.2 mainshock and (b) the M_w 5.6 aftershock Christchurch earthquakes. Columns represent the simulated values of *Fp* and vertical and horizontal peak accelerations, respectively. Horizontal solid lines indicate *Fp* and peak accelerations obtained from the observed waveforms, and horizontal dotted lines show corresponding values from the input motions (Fig. 7). The best-fitting parameters are marked by black squares, which are chosen such that the simulated *Fp* and peak accelerations agree with the data from both the mainshock and aftershock. The color version of this figure is available only in the electronic edition.

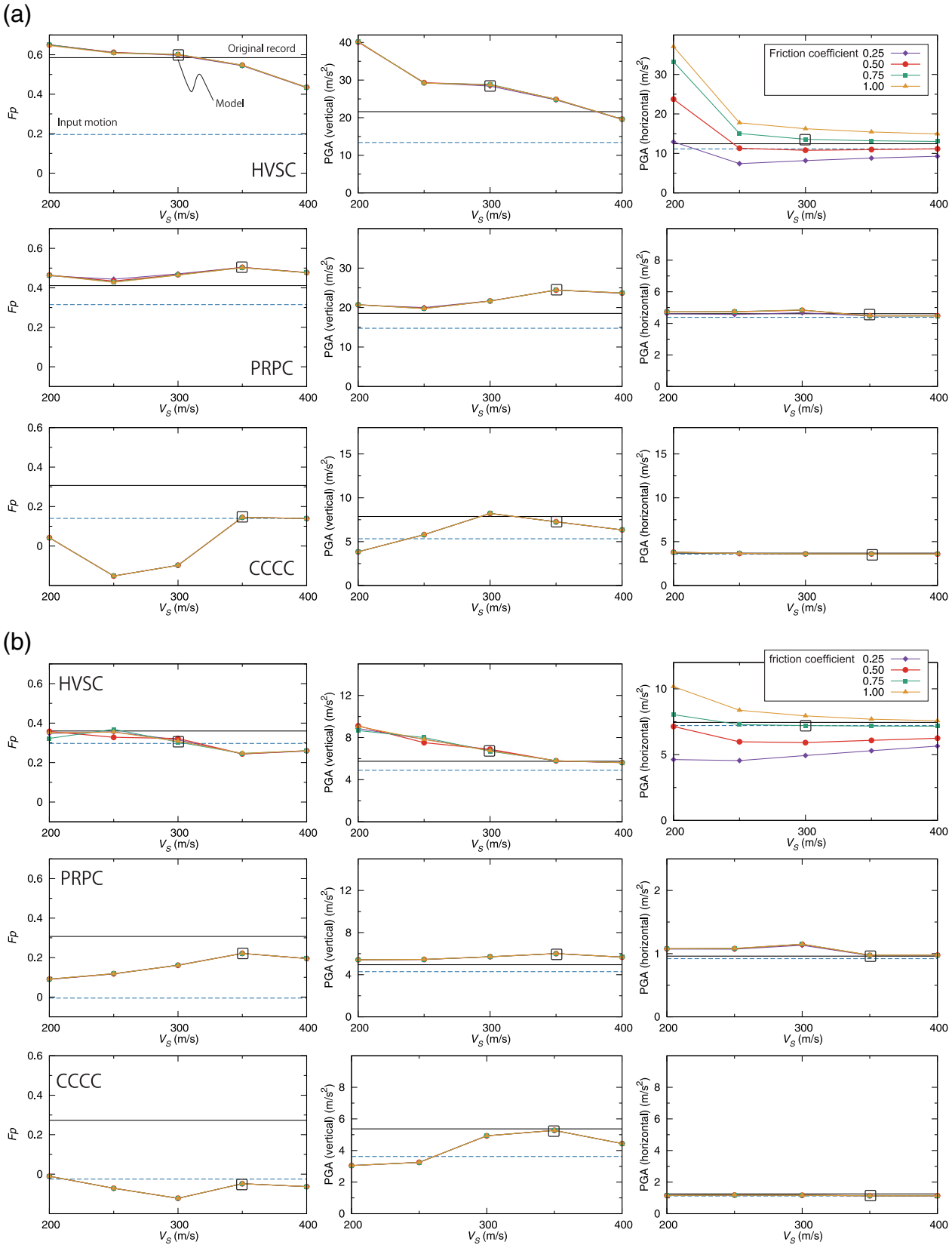

Figure A2. Dependence of *S*-wave velocity and friction coefficients on the resulting waveform asymmetry and peak accelerations. A simulated AsVA is characterized by *Fp* and vertical and horizontal peak accelerations during (a) the 2011 M_w 6.2 mainshock and (b) the M_w 5.6 aftershock Christchurch earthquakes. Columns represent the simulated values of *Fp* and vertical and horizontal peak accelerations, respectively. Horizontal solid lines indicate *Fp* and peak accelerations obtained from the observed waveforms, dotted lines show corresponding values from the input motions (Fig. 7). The best-fitting parameters are marked by black squares. The color version of this figure is available only in the electronic edition.